



ELSEVIER

journal homepage: www.elsevier.com/locate/jmatprotec

Effect of antimony substitution on structural and electrical properties of LaFeO₃

L. John Berchmans^{a,*}, R. Sindhu^b, S. Angappan^a, C.O. Augustin^a

^a Central Electrochemical Research Institute, Karaikudi 630006, India

^b Department of Materials Science, Madurai Kamaraj University, Madurai-625021, India

ARTICLE INFO

Keywords:

Perovskites

Co-precipitation

X-ray diffraction

Conductivity

ABSTRACT

Fine crystalline LaFeO₃ and antimony-substituted compounds have been prepared by co-precipitation method. The as synthesized materials have been sintered at 1000 °C for single-phase compound formation and evaluated for their electrical and structural properties. TG/DTA studies ascribed that the precursor powders have undergone rapid changes during the transformation of LaFeO₃ and substituted compounds. XRD data reveal the presence of well-defined sharp peaks, indicating the single-phase perovskite structure of LaFeO₃ and polycrystalline structure of LaFeO₃ and Sb₂O₃ compounds. The FT-IR spectra exhibit an absorption band corresponding to Fe–O stretching vibration, which is shifted on the substitution of Sb³⁺ ions. The temperature dependent d.c. conductivity shows the semiconducting behavior of the synthesized materials. The band gap values are found to increase upto $x=0.4$ and decrease on further increase in concentrations of the Sb³⁺ ions. The decrease in dielectric constant with increasing frequency explained the Maxwell–Wagner Interfacial polarization model.

© 2008 Published by Elsevier B.V.

1. Introduction

Perovskite oxides with the general formula of ABO₃ structure have received considerable attention owing to their potential applications such as catalysts (Delmastro et al., 2001), sensors (Shimizu et al., 1985), fuel cells (Minh, 1993), and environmental monitoring systems (Martinelli et al., 1999) etc. Among the perovskite oxides, LaFeO₃ and A and B-site substituted LaFeO₃ with the general formula of La_{1-x}A_xFeO₃ and LaFe_{1-x}B_xO₃ (where A = Ce, Sr, Sm or other rare earth elements and B = Cr, Co or other transition metals) have been studied because of their extensive usage in various technological applications. Due to their stability, sensitivity and selectivity of these materials they are used as e-noses for diagnosis of the diseases using the gas-sensing properties (Zhang et al., 2006). The structural and electrical properties of these materials are

strongly depending on the methods of preparation including hydrothermal process (Zheng et al., 2000), combustion synthesis (Manoharan and Patil, 1993), sol-gel method (Spinicci et al., 2002), co-precipitation (Li et al., 1999) and citrate gel process (Li et al., 1994).

Recently, the perovskite oxides of SrFeO₃ (Augustin et al., 2004) and La_xSr_{1-x}FeO₃ (Augustin et al., 2005) have been proposed as potential electrodes in metallurgical applications for the replacement of conventionally used carbon anodes due to their high temperature stability, high electrical conductivity and chemical stability. In this regard, this communication envisages the structural, electrical and morphological features of Sb³⁺ substituted LaFeO₃ using co-precipitation method. As far as our knowledge goes no one has attended the detailed characterization of different properties like electrical conductivity by bipolaron conduction on Sb³⁺ ions (Brahma et al.,

* Corresponding author.

E-mail address: ljberchmans@yahoo.com (L. John Berchmans).
0924-0136/\$ – see front matter © 2008 Published by Elsevier B.V.
doi:10.1016/j.jmatprotec.2008.06.054

2000), thermal stability via sintering kinetics on antimony substitution (Shi et al., 2003), the study has been carried out in detail and presented in this paper.

2. Experimental

Co-precipitation method was employed for the preparation of sub micron sized $\text{La}_{1-x}\text{Sb}_x\text{FeO}_3$ ($x=0.0, 0.2, 0.4, 0.6, 0.8$) powders using analytical grade $\text{La}(\text{NO}_3)_3 \cdot 6\text{H}_2\text{O}$, $\text{Fe}(\text{NO}_3)_3 \cdot 9\text{H}_2\text{O}$, SbCl_3 and NaOH as starting materials. Stoichiometric quantities of starting materials were dissolved in deionised water to get a homogeneous mixture of nitrate and chloride solution. To form the precipitate NaOH solution was added to the mixture in drop wise, until the resulting suspension reached the pH of 9. Then the suspension was heated to 60°C with continuous stirring to promote the precipitation reaction. The precipitate was then filtered through a filtering medium using a vacuum pump. The filtered mass was washed repeatedly with deionised water under warm conditions until the entire NaNO_3 was removed from the precipitate and finally rinsed with rectified spirit. "Brown ring test" was carried out to confirm the absence of nitrates. Then the precipitate was dried at 100°C for few hours to get the moisture free powders. The powders were finely ground and sintered at 1000°C to promote the compound formation. Differential thermal analysis and thermogravimetry (DTA/TG, Rigaku Thermalplus, TG 8120) were used to study the phase transition of green and sintered powders. A heating rate of $10^\circ\text{C}/\text{min}$ was used for the measurements from room temperature to 900°C in air. The sintered powders were examined for their crystallinity by X-ray powder diffraction (XRD) patterns using $\text{Cu K}\alpha$ ($\alpha = 1.541 \text{ \AA}$) radiation with 2θ values ranging from 10° to 80° in JEOL8030 X-ray diffractometer. FT-IR spectra were recorded using Perkin Elmer UK-Paragon-500 spectrophotometer. DC electrical conductivity was measured using a four probe method from room temperature to 1000°C . AC electrical conductivity was determined from 50 Hz to 10 kHz with the help of a computerized LCRTZ test system (CLCRTZIP-Model). The dielectric constant and dielectric loss tangent of the samples were also calculated. The morphological studies were carried out using a scanning electron microscope JEOL (JSM-35 CF) instrument.

3. Results and discussion

Fine particles of LaFeO_3 and substituted compounds were obtained from aqueous solutions of lanthanum nitrate, ferric nitrate and antimony chloride. During the process of co-precipitation, nucleation occurs by the addition of NaOH solution, producing fine crystallites of $\text{La}_{1-x}\text{Sb}_x\text{FeO}_3$ compounds. The metal cations are dispersed in the suspension and converted into their hydroxides in the form of colloidal particles. The following are the reactions takes place during chemical precipitate process (Augustin et al., 2004).

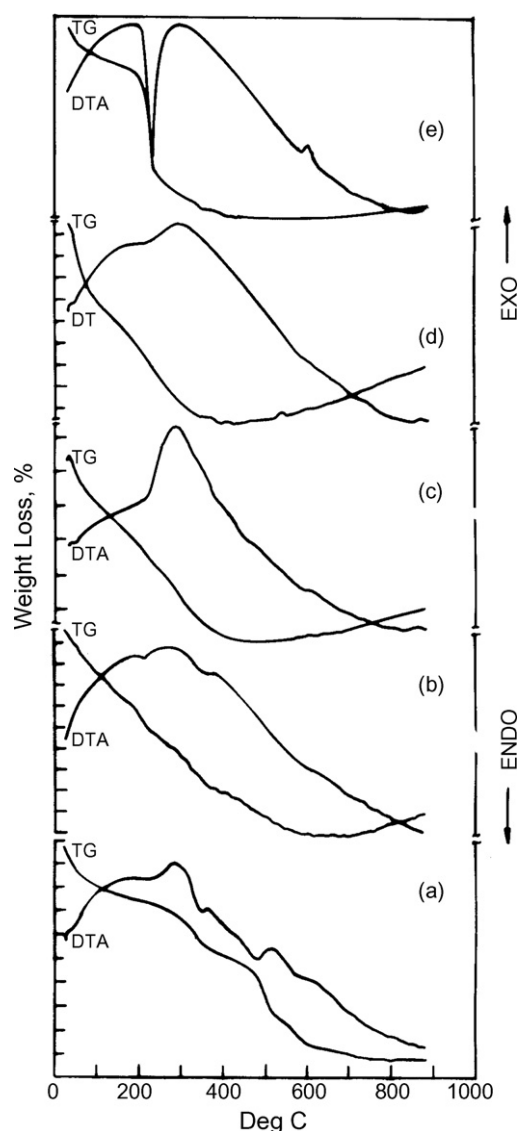
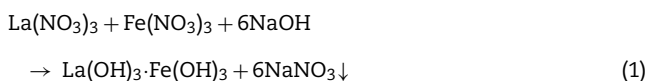


Fig. 1 – DTA/TG curve of $\text{La}_{1-x}\text{Sb}_x\text{FeO}_3$ (a) $x=0.0$, (b) $x=0.2$, (c) $x=0.4$, (d) $x=0.6$, (e) $x=0.8$.

The above precursor is subjected to heating which transform the metal hydroxides to ferrite compounds.

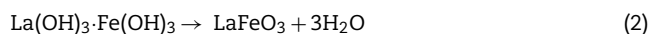


Fig. 1 shows the TG/DTA curves of as synthesized $\text{La}_{1-x}\text{Sb}_x\text{FeO}_3$ ($x=0.0, 0.2, 0.4, 0.6, 0.8$) compounds with a heating rate of $10^\circ\text{C}/\text{min}$. The TG curve of LaFeO_3 shows two weight losses, one is at $180\text{--}230^\circ\text{C}$ and another at $290\text{--}470^\circ\text{C}$ respectively. The former weight loss reveals the fact that the loss of water during the process of dehydration and the later is mainly due to the decomposition of nitrate molecules and the release of other gases. Beyond 600°C , it is observed that there is no prominent changes occurred in the TG/DTA curves, which elucidates the initiation of the compound formation starts at this temperature. This observation is also been reflected in the DTA curve exhibiting an exothermic peak around 600°C . This indicates that the precursor powders have undergone rapid

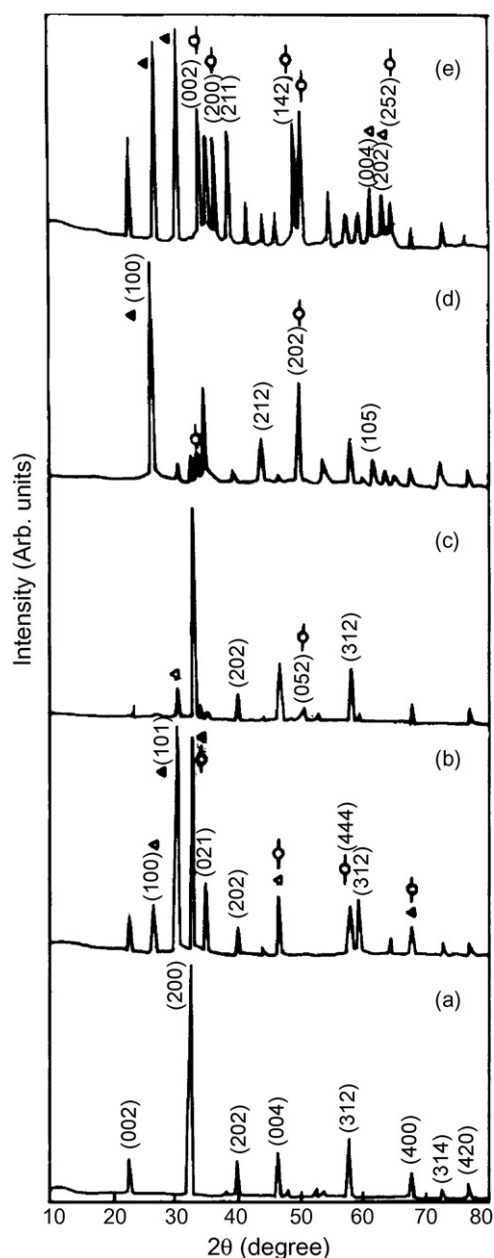


Fig. 2 – XRD patterns of $\text{La}_{1-x}\text{Sb}_x\text{FeO}_3$ (a) $x=0.0$, (b) $x=0.2$, (c) $x=0.4$, (d) $x=0.6$ and (e) $x=0.8$: (Δ) La_2O_3 , (\circ) Sb_2O_3 , (\blacktriangle) LaSbFeO_3 .

chemical changes and forming LaFeO_3 . From the TG curve of Sb^{3+} substituted LaFeO_3 , the temperature for the compound formation is increases with increasing concentration of Sb^{3+} . There is no prominent exo/endothemic peaks are observed in the substituted ferrite samples.

Fig. 2 shows the XRD patterns of $\text{La}_{1-x}\text{Sb}_x\text{FeO}_3$ ($x=0.0, 0.2, 0.4, 0.6, 0.8$) sub micron sized particles sintered at 1000°C . The well-defined sharp peaks of LaFeO_3 elucidate that the single-phase compound formation of orthorhombic perovskite structure with the lattice parameters of $a=5.539\text{ \AA}$, $b=5.561\text{ \AA}$ and $c=7.836\text{ \AA}$. The lattice parameter values of substituted ferrites are given in Table 1. All the samples with and without antimony substitution exhibit the orthorhombic

Table 1 – XRD lattice parameters

Compounds	a (\AA)	b (\AA)	c (\AA)
LaFeO_3	5.539	5.561	7.836
$\text{La}_{0.8}\text{Sb}_{0.2}\text{FeO}_3$	5.529	5.415	7.847
$\text{La}_{0.6}\text{Sb}_{0.4}\text{FeO}_3$	5.539	5.548	7.819
$\text{La}_{0.4}\text{Sb}_{0.6}\text{FeO}_3$	5.482	5.446	7.876
$\text{La}_{0.2}\text{Sb}_{0.8}\text{FeO}_3$	5.514	5.497	7.908

structure, which is confirmed by the peak positions of XRD. On increasing the concentrations of Sb^{3+} ions $x \geq 0.4$, a sharp increase in the peak positions is observed. It is also seen that the decrease in lattice constants with increase in concentrations of the Sb^{3+} ions may be due to the smaller ionic radii of Sb^{3+} ions ($r_{\text{Sb}^{3+}}=0.76\text{ \AA}$) in place of La^{3+} ions ($r_{\text{La}^{3+}}=1.02\text{ \AA}$) (Shannon, 1976; Thangadurai et al., 2002). In addition to the single-phase perovskite structure some secondary phases of Sb_2O_3 peaks exist on higher concentrations confirms the solubility limit of Sb^{3+} is well within the limit of $x=0.6$.

The FT-IR spectra of $\text{La}_{1-x}\text{Sb}_x\text{FeO}_3$ ($x=0.0, 0.2, 0.4, 0.6, 0.8$) particles sintered at 1000°C measured in the frequency range of $400\text{--}1000\text{ cm}^{-1}$ are shown in Fig. 3(a–e). The spectrum for the parent LaFeO_3 shows an absorption band at 565.46 cm^{-1} corresponds to Fe-O stretching vibration and $\gamma\text{Fe-O}$. This value

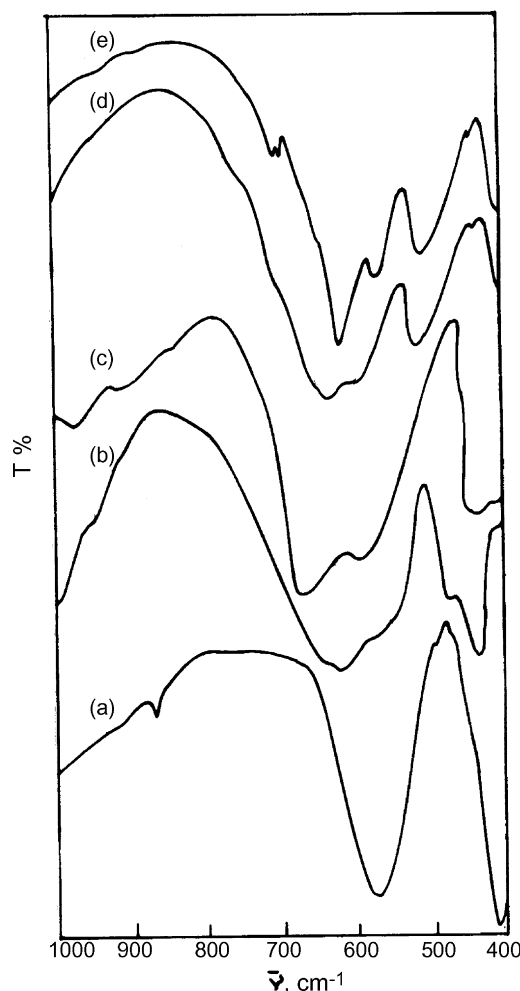


Fig. 3 – FTIR spectra of $\text{La}_{1-x}\text{Sb}_x\text{FeO}_3$ (a) $x=0.0$, (b) $x=0.2$, (c) $x=0.4$, (d) $x=0.6$, (e) $x=0.8$.

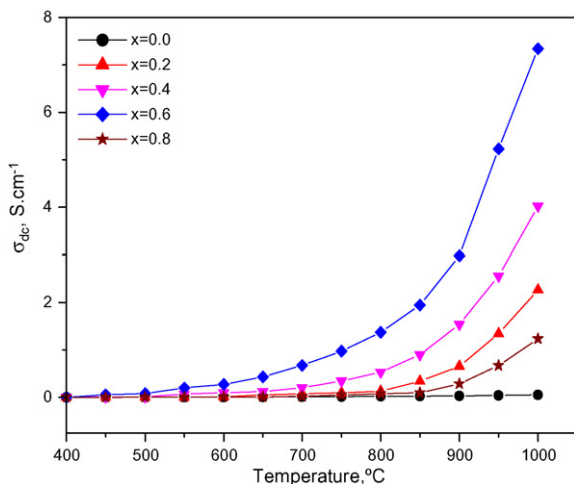


Fig. 4 – DC conductivity vs temperature for $\text{La}_{1-x}\text{Sb}_x\text{FeO}_3$.

of $\gamma\text{Fe-O}$ may be attributed to the stretching vibration of metal cations situated in the octahedral site. On substitution with Sb^{3+} ions where $x=0.2$ multiple absorption bands occur and also the $\gamma\text{Fe-O}$ bands are shifted from 565.46 cm^{-1} to 652.36 cm^{-1} . On further increase in concentration of Sb^{3+} ions where $x=0.4$, a more shift is noticed on the band position. It is well known that the cation in the octahedral site usually possesses two IR active modes, which is also reflected in the spectra. The observed absorption peak values are well consistent with the previous literature (Porta et al., 2001).

DC electrical conductivity of LaFeO_3 and Sb^{3+} ions and substituted compounds with different concentrations of Sb^{3+} ions is shown in Fig. 4. It is seen that the conductivity values of all the synthesized materials are found to increase with increase in measuring temperature, which infers the conduction mechanism is changed from insulating to semiconducting behavior. At lower temperature, the conduction is due to electronic conduction whereas at higher temperatures the conduction may be due to ionic conduction. The maximum conductivity for LaFeO_3 is found to be 1.004 S cm^{-1} measured at 1000°C , for the samples sintered at 1000°C . In general the conductivity of the compound mainly depends upon the presence of holes, electrons and ionic concentrations in the compound. The conducting mechanism of the synthesized LaFeO_3 can be assigned to the following redox reaction



As the substitution of Sb^{3+} ions increases, the conductivity also found to increase up to $x=0.6$ and thereafter it decreases. The maximum electrical conductivity of 7.3 S cm^{-1} was observed for $\text{La}_{0.4}\text{Sb}_{0.6}\text{FeO}_3$. It is resulted from the contribution of the increased charge carriers due to the bi-polaron transition of $\text{Sb}^{5+}/\text{Sb}^{3+}$ ions (Brahma et al., 2000). The following are the redox reaction mechanism and may be given by the equation.

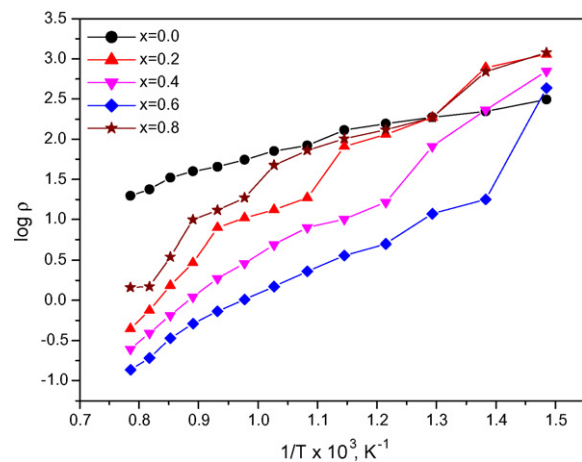


Fig. 5 – Arrhenius plot of $\text{La}_{1-x}\text{Sb}_x\text{FeO}_3$.

At higher concentration of Sb^{3+} ions in the parent LaFeO_3 ($x=0.8$) the conductivity values are found to decrease because of the enhanced distortion of the structure and disorder scattering of holes (Williams and Ryan, 2001).

Fig. 5 shows the Arrhenius plot of ($\log \rho$ vs $1/T \times 10^3$) for $\text{La}_{1-x}\text{Sb}_x\text{FeO}_3$ sintered at 1000°C calculated from the following equation

$$(6) \rho = \rho_0 \exp\left(\frac{E_a}{KT}\right)$$

where E_a is the activation energy of the conduction process, K is the Boltzmann constant and T is the absolute temperature. With the increase in substitution of Sb^{3+} ions, a linear increase in conductivity is noticed. This observation is in good agreement with the reported values of many other electronically conductive perovskite systems. (Stevenson et al., 1993, 1996; Tai et al., 1995; Kuo et al., 1990).

From the activation energies (Table 2), it is noticed that the existence of the lower slope in the curves resulted due to the lower activation energy in the compound. This observation suggests that the electronic conduction is more predominant at the lower temperature region, whereas at higher temperatures the change in slope of the curve indicating that the conduction mechanism changes from electronic to ionic conduction. It increases rapidly with increasing temperature due to the higher activation energy prevails in the system as reported in the case of CSGM perovskite system (Stevenson et al., 2000). The band gap (E_g) values are calculated from the graph $\log \rho$ vs $1/T$ using the relation $E_g = \text{slope} \times 2.303K$. From the E_g values, it is seen that the values are found to increase

Table 2 – Activation energy

Compounds	Activation energy (eV)	
	Lower temperature	Higher temperature
LaFeO_3	0.92	0.721
$\text{La}_{0.8}\text{Sb}_{0.2}\text{FeO}_3$	0.75	0.640
$\text{La}_{0.6}\text{Sb}_{0.4}\text{FeO}_3$	0.68	0.538
$\text{La}_{0.4}\text{Sb}_{0.6}\text{FeO}_3$	0.47	0.417
$\text{La}_{0.2}\text{Sb}_{0.8}\text{FeO}_3$	1.20	1.609

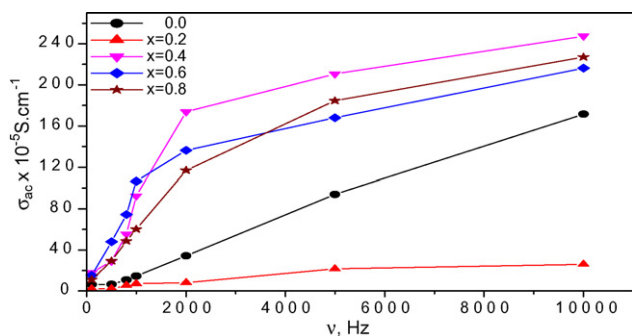


Fig. 6 – AC conductivity vs frequency for $\text{La}_{1-x}\text{Sb}_x\text{FeO}_3$.

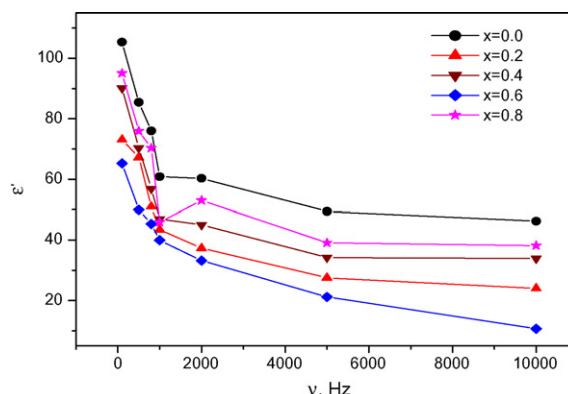


Fig. 7 – Dielectric constant vs frequency for $\text{La}_{1-x}\text{Sb}_x\text{FeO}_3$.

on the substitution of Sb^{3+} ions in the compound and decrease on further increase in the concentrations. The maximum band gap of 1.609 eV is observed for compounds where $x = 0.8$.

The dependence on the AC electrical conductivity of the synthesized compounds $\text{La}_{1-x}\text{Sb}_x\text{FeO}_3$ ($x = 0.0, 0.2, 0.4, 0.6, 0.8$) are presented in Fig. 6. Since the increase in frequency enhances the hopping frequency of the charge carriers Fe^{2+} and Fe^{3+} , the conductivity is increased. The conduction mechanism of ferrite is explained on the basis of hopping of charge carriers between the Fe^{2+} and Fe^{3+} ions. The compositional dependence on AC conductivity also increases with the addition of Sb^{3+} ion in various molar proportions except $x = 0.2$.

For all the samples, the frequency dependent behaviour is noticed, where the dielectric constant decreases with increase in frequency (Fig. 7). It is revealed that the numbers of ferrous ions in the octahedral sites, which are taking part in the electron exchange interaction Fe^{2+} to Fe^{3+} , are responsible for polarization, as reported in many of the ferrite materials (Soliman Selim et al., 1999). The decrease in dielectric constant with increasing frequency can be explained on the basis of Maxwell-Wagner interfacial polarization model (Wagner, 1913). According to Maxwell-Wagner model the dielectric structure of a ferrite compound is made up of two layers. The first layer being a conducting layer consists of large ferrite grains and the other being grain boundaries, which are said to be poor conductors. The polarization appears due to an electronic exchange between the ferrous and ferric ions, produced by the local displacements in the direction of the applied field. The decrease in dielectric constant with increase in frequency may be due to the presence of ferric ions.

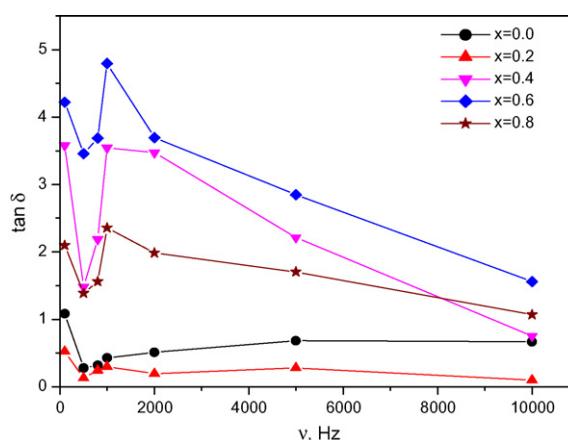


Fig. 8 – Loss tangent vs frequency for $\text{La}_{1-x}\text{Sb}_x\text{FeO}_3$.

Fig. 8 shows the variation of loss tangent with frequency for the samples LaFeO_3 ($x = 0.0, 0.2, 0.4, 0.6, 0.8$). It can be seen that the values of $\tan \delta$ are found to decrease with the presence of Sb^{3+} ions in the parent compounds. It is also noticed that an abnormal dielectric behavior was observed for all the samples because the dielectric relaxation peaks are resulted at a frequency of 1 kHz. According to Rezlescu model the relaxation peaks may be due to the collective contribution of both p- and n-type charge carriers (John Berchmans et al., 2004). The electronic exchange between Fe^{3+} and Fe^{2+} and the hole transfer between Sb^{3+} and Sb^{5+} are responsible for such behavior. Furthermore the jumping frequencies of localized charge

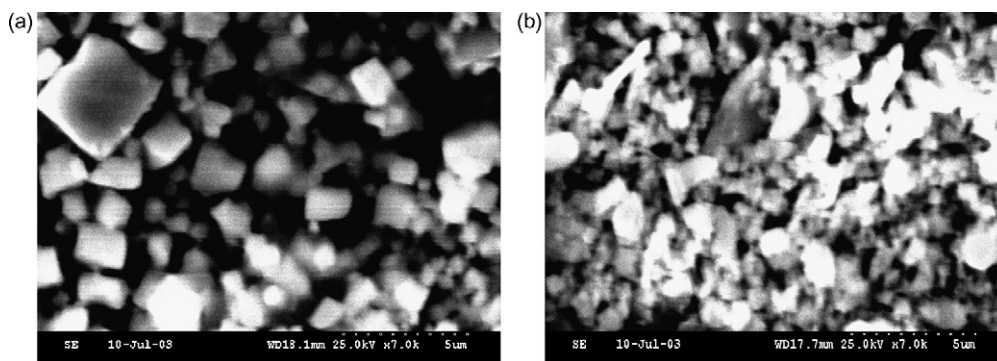


Fig. 9 – SEM images of $\text{La}_{1-x}\text{Sb}_x\text{FeO}_3$: (a) $x = 0.0$, (b) $x = 0.2$.

carriers are almost equal to that of the applied AC electric field

The SEM images of LaFeO_3 and $\text{La}_{0.8}\text{Sb}_{0.2}\text{FeO}_3$ are shown in Fig. 9(a) and (b). It is evident that the material exhibits the presence of fine grain size particles with irregular shape. Fig. 9(a) shows the well-defined crystals with poor inter-grain connectivity over the scanned area of the synthesized compounds. The introduction of Sb^{3+} ions (Fig. 9 (b)) influences the fine crystallite formation, which may be resulted in the change in the electrical properties of the materials due to their grain-to-grain connectivity.

4. Conclusion

The co-precipitation is one of the simplest and novel method to prepare LaFeO_3 and substituted compounds. TG/DTA curves show the thermochemical behaviour of the compound with respect to temperatures. XRD patterns reveal the single-phase compound formation with and without antimony substitution, exhibiting the orthorhombic structure. FTIR spectra show the absorption bands for Fe–O and γFe –O stretching vibrations for the above compounds. The electrical conductivity of the synthesized LaFeO_3 and substituted compounds are found to increase with increasing measuring temperature. AC electrical conductivity shows that the dielectric constant is found to decrease with increase in frequency. The SEM images reveal the presence of fine crystallites formation of the parent and substituted compounds of LaFeO_3 .

Acknowledgements

The authors express their gratitude to the Director, CECRI, and staff, Department of Metallurgy for their kind help.

REFERENCES

- Augustin, C.O., John Berchmans, L., Kalai Selvan, R., 2004. Structural electrical and electrochemical properties of co-precipitated $\text{SrFeO}_{3-\delta}$. *Mater. Lett.* 58, 1260–1266.
- Augustin, C.O., Kalai Selvan, R., Nagaraj, R., John Berchmans, L., 2005. Effect of La^{3+} substitution on the structural, electrical and electrochemical properties of strontium ferrite by citrate combustion method. *Mater. Chem. Phys.* 89, 406–411.
- Brahma, P., Banerjee, S., Chakraborty, S., Chakravorty, D., 2000. Small polaron and bipolaron transport in antimony oxide doped barium hexaferrites. *J. Appl. Phys.* 88, 6526–6528.
- Delmastro, A., Mazza, D., Ronchetti, S., Vallino, M., Spinicci, R., Broveto, P., Salis, M., 2001. Synthesis and characterization of non-stoichiometric LaFeO_3 perovskite. *Mater. Sci. Eng. B* 79, 140–145.
- John Berchmans, L., Kalai Selvan, R., Selva Kumar, P.N., Augustin, C.O., 2004. Structural and electrical properties of $\text{Ni}_{1-x}\text{Mg}_x\text{Fe}_2\text{O}_4$ synthesised by citrate gel process. *J. Magn. Mater.* 279, 103–110.
- Kuo, J.H., Anderson, H.U., Sparlin, D.M., 1990. Oxidation-reduction behaviour of undoped and Sr-doped LaMnO_3 : defect structure, electrical conductivity and thermoelectric power. *J. Solid State Chem.* 87, 55–63.
- Li, K., Wang, D., Wu, F., Xie, T., Li, T., 1999. Studies on photoelectric gas-sensitive characters of nanocrystalline LaFeO_3 . *Mater. Chem. Phys.* 60, 226–230.
- Li, X., Zhang, H., Zhao, M., 1994. Preparation of nanocrystalline LaFeO_3 using reverse drop coprecipitation with polyvinyl alcohol as protecting agent. *Mater. Chem. Phys.* 37, 132–135.
- Manoharan, S.S., Patil, K.C., 1993. Combustion route to fine particle perovskite oxides. *J. Solid State Chem.* 102, 267–276.
- Martinelli, G., Carotta, M.C., Ferrini, M., Sadaoka, Y., Traversa, E., 1999. Screen-printed perovskite-type thick films as gas sensors for environmental monitoring. *Sens. Actuators B* 55, 99–110.
- Minh, N.Q., 1993. Ceramic fuel cells. *J. Am. Ceram. Soc.* 76, 563–588.
- Porta, P., Cimino, S., Rossi, S.D., Faticanti, M., Minelli, G., Pettiti, I., 2001. AFeO_3 (A = La, Nd, Sm) and $\text{LaFe}_{1-x}\text{Mg}_x\text{O}_3$ perovskites: structural and redox properties. *Mater. Chem. Phys.* 71, 165–173.
- Shannon, R.D., 1976. Revised effective ionic radii and systematic studies of interatomic distances in halides and chalcogenides. *Acta Crystallogr. A* 32, 751–767.
- Shi, L., Li, G., Feng, S.J., Li, X.G., 2003. Effect of Sb doping on the structure and transport properties of the Ru-1222 system. *Phys. Stat. Sol. (a)* 198, 137–141.
- Shimizu, Y., Shimabukuro, M., Arai, H., Seiyama, T., 1985. Enhancement of humidity sensitivity for perovskite-type oxides having semiconductivity. *Chem. Lett.* 14, 917–920.
- Soliman Selim, M., Turkey, G., Shouman, M.A., El-Shobaky, G.A., 1999. Effect of Li_2O doping on electrical properties of CoFe_2O_4 . *Solid State Ionics* 120, 173–181.
- Spinicci, R., Tofanari, A., Delmastro, A., Mazz, D., Ronchetti, S., 2002. Catalytic properties of stoichiometric and non-stoichiometric LaFeO_3 perovskite for total oxidation of methane. *Mater. Chem. Phys.* 76, 20–25.
- Stevenson, J.W., Nasrallah, M.M., Anderson, H.U., Sparlin, D.M., 1993. Defect structure of $\text{Y}_{1-y}\text{Ca}_y\text{MnO}_3$ and $\text{La}_{1-y}\text{Ca}_y\text{MnO}_3$. I. Electrical properties. *J. Solid State Chem.* 102, 175–184.
- Stevenson, J.W., Armstrong, T.R., Carneim, R.D., Pederson, L.R., Weber, W.J., 1996. Electrochemical properties of mixed conducting perovskites $\text{La}_{1-x}\text{M}_x\text{Co}_{1-y}\text{Fe}_y\text{O}_{3-\delta}$ (M = Sr, Ba, Ca). *J. Electrochem. Soc.* 143, 2722–2729.
- Stevenson, J.W., Hasinska, K., Canfield, N.L., Armstrong, T.R., 2000. Influence of cobalt and iron additions on the electrical and thermal properties of (La, Sr) (Ga, Mg) $\text{O}_{3-\delta}$. *J. Electrochem. Soc.* 147, 3213–3218.
- Thangadurai, V., Beurmann, P.S., Weppner, W., 2002. $\text{SrSn}_{1-x}\text{Fe}_x\text{O}_{3-\delta}$ ($0 < x < 1$) perovskites: a novel mixed oxide ion and electronic conductor. *Mater. Res. Bull.* 37, 599–604.
- Tai, L.W., Nasrallah, M.M., Anderson, H.U., Sparlin, D.M., Sehlin, S.R., 1995. Structure and electrical properties of $\text{La}_{1-x}\text{Sr}_x\text{Co}_{1-y}\text{Fe}_y\text{O}_3$. Part 2. The system $\text{La}_{1-x}\text{Sr}_x\text{Co}_{0.2}\text{Fe}_{0.8}\text{O}_3$. *Solid State Ionics* 76, 273–283.
- Wagner, K.W., 1913. Zur theorie der unvollkommenen dielektrika. *Ann. Phys.* 40, 817–855.
- Williams, G.V., Ryan, M., 2001. Raman transport and magnetization study of the $\text{RuSr}_2\text{R}_{2-x}\text{Ce}_x\text{Cu}_2\text{O}_{10+\delta}$ (R = Gd, Eu) high-temperature superconducting cuprates. *Phys. Rev. B* 64, 1–8, 094515.
- Zhang, L., Qin, H., Song, P., Hu, J., Jiang, M., 2006. Electric properties and acetone-sensing characteristics of $\text{La}_{1-x}\text{Pb}_x\text{FeO}_3$ perovskite system. *Mater. Chem. Phys.* 98, 358–362.
- Zheng, W., Liu, R., Peng, D., Meng, G., 2000. Hydrothermal synthesis of LaFeO_3 under carbonate-containing medium. *Mater. Lett.* 43, 19–22.